Cell Motility and the Cytoskeleton 59:227–241 (2004)

Sphingosine-1-Phosphate Plays a Role in the Suppression of Lateral Pseudopod Formation During *Dictyostelium discoideum* Cell Migration and Chemotaxis

Akhilesh Kumar,[1] Deborah Wessels,[1] Karla J. Daniels,[1] Hannah Alexander,[1] Stephen Alexander,[2] and David R. Soll[1]

[1]*W.M. Keck Dynamic Image Analysis Facility, Department of Biological Sciences, The University of Iowa, Iowa City*

[2]*Division of Biological Sciences, University of Missouri, Columbia*

Sphingosine-1-phosphate (S-1-P) is a bioactive lipid that plays a role in diverse biological processes. It functions both as an extracellular ligand through a family of high-affinity G-protein-coupled receptors, and intracellularly as a second messenger. A growing body of evidence has implicated S-1-P in controlling cell movement and chemotaxis in cultured mammalian cells. Mutant *D. discoideum* cells, in which the gene encoding the S-1-P lyase had been specifically disrupted by homologous recombination, previously were shown to be defective in pseudopod formation, suggesting that a resulting defect might exist in motility and/or chemotaxis. To test this prediction, we analyzed the behavior of mutant cells in buffer, and in both spatial and temporal gradients of the chemoattractant cAMP, using computer-assisted 2-D and 3-D motion analysis systems. Under all conditions, S-1-P lyase null mutants were unable to suppress lateral pseudopod formation like wild-type control cells. This resulted in a reduction in velocity in buffer and spatial gradients of cAMP. Mutant cells exhibited positive chemotaxis in spatial gradients of cAMP, but did so with lowered efficiency, again because of their inability to suppress lateral pseudopod formation. Mutant cells responded normally to simulated temporal waves of cAMP but mimicked the temporal dynamics of natural chemotactic waves. The effect must be intracellular since no homologs of the S-1-P receptors have been identified in the *Dictyostelium* genome. The defects in the S-1-P lyase null mutants were similar to those seen in mutants lacking the genes for myosin IA, myosin IB, and clathrin, indicating that S-1-P signaling may play a role in modulating the activity or organization of these cytoskeletal elements in the regulation of lateral pseudopod formation. Cell Motil. Cytoskeleton 59:227–241, 2004. © 2004 Wiley-Liss, Inc.

Key words: sphingosine 1-phosphate lyase; cell motility; pseudopod formation; cell polarity; ceramide; EDG/S1P receptors; G-protein coupled receptors

INTRODUCTION

Sphingosine-1-phosphate (S-1-P), an intermediate metabolite of sphingomyelin degradation, is a bioactive lipid that functions in signal transduction and has been demonstrated to play a role in the regulation of a variety of cellular processes [Pyne and Pyne, 2000; Spiegel, 1999; Spiegel and Milstien, 2002; Saba and Hla, 2004]. The cellular level of S-1-P is controlled by the combined action of sphingosine kinases, which phosphorylate sphingosine to produce S-1-P, S-1-P phosphatases, which dephosphorylate S-1-P and S-1-P lyase, which degrades S-1-P to hexadecanal and phosphoethanolamine.

In animal cells, S-1-P acts as an extracellular signaling molecule as well as an intracellular second mes-

Contract grant sponsor: NIH; Contract grant numbers: HD-18577 and GM53929.

*Correspondence to: Dr. David R. Soll, Department of Biological Sciences, 302 BBE, The University of Iowa, Iowa City, IA 52242. E-mail: david-soll@uiowa.edu

Received 25 June 2004; accepted 17 August 2004

Published online in Wiley InterScience (www.interscience.wiley.com).
DOI: 10.1002/cm.20035

senger [Spiegel, 2000; Spiegel and Milstien, 2000]. As an extracellular ligand, S-1-P signals through a family of at least 5 high-affinity G-protein-coupled, membrane spanning EDG (endothelial differentiation growth) receptors (now referred to as S1P receptors). Receptor-mediated S-1-P signaling has been shown to mediate the motility and chemoinvasivness of several cell types, as well as activate MAP kinases and cell proliferation [Wu et al., 1995; Pyne and Pyne, 1996]. Intracellular S-1-P functions in suppressing apoptosis [Cuvillier et al., 1996; Cuvillier and Levade, 2001; Machwate et al., 1998] and regulating Ca^{2+} homeostasis [Okamoto et al., 1998; Van Brocklyn et al., 1998] in a variety of cell types.

Numerous reports have implicated S-1-P in the regulation of cell motility and metastasis [Spiegel et al., 2002]. Signaling through different EDG/S1P receptors has been shown to either increase or decrease cell movement in a Rac- and Rho-dependent manner [Okamoto et al., 2000]. Exogenously added S-1-P has been shown to inhibit the motility and chemotactic invasiveness of B16 mouse melanoma cells through Matrigel [Sadahira et al., 1992; Yamamura et al., 1997] and of estrogen-independent human MDA-MB-231 invasive breast cancer cells [Wang et al., 1999; Sliva et al., 2000]. In addition, S-1-P has been shown to promote endothelial cell migration [Lee et al., 1999; Kimura et al., 2000; Boguslawski et al., 2002], but to inhibit smooth muscle cell migration [Boguslawski et al., 2002]. In some cases, the changes in cell behavior have been shown to be accompanied by a reduction in F-actin nucleation and lamellae formation [Bornfeldt et al., 1995; Yamamura et al., 1996].

A more precise understanding of the role S-1-P plays in motility and chemotaxis requires an experimental system in which there is a well-developed empirical and theoretical framework for the regulation of cell motility and chemotaxis, and the opportunity to specifically delete and over-express genes that regulate the synthesis and degradation of S-1-P. Employing *Dictyostelium discoideum* to study the role of S-1-P in motility and chemotaxis has several advantages. First, the signal transduction pathways that regulate receptor-mediated cell behavior in the different phases of the relayed chemotactic wave have been described in more detail [Laub and Loomis, 1998; Firtel and Chung, 2000] than in other eukaryotes because of the ease in generating null mutants [DeLozanne and Spudich, 1987] as a result of the haploid nature of *D. discoideum* [Kessin, 2001; Kuspa and Loomis, 1994]. Second, a set of experimental protocols has been developed to assess the basic motile behavior of cells in the absence of chemoattractant, and the behavioral responses to the spatial, temporal and concentration components of the four phases of the natural chemotactic wave [Soll et al., 2003]. Third, the behavior of *D. discoideum* has been quantitatively described in more detail in 2D and 3D using computer-assisted methods [Soll, 1995; Soll and Voss, 1998; Soll et al., 2000] than the behavior of any other amoeboid cell type.

A *D. discoideum* mutant in which the sphingosine lyase gene (*sglA*) was deleted by homologous recombination (*sglA*Δ) exhibited a number of defects in development [Li et al., 2001]. These included defects in (1) cell morphology and pseudopod formation, (2) the migration of multicellular slugs towards light, (3) expression of developmentally controlled genes in slugs, (4) developmental timing, and (5) the production of normal numbers of spores. The defects in cellular morphology and pseudopod formation suggested that the S-1-P lyase mutant might be defective in motility and/or chemotaxis. Therefore, using computer-assisted 2D and 3D motion analysis systems, we analyzed two independently generated S-1-P lyase null mutants for basic cell motility in the absence of chemoattractant, in response to spatial gradients of attractant, and in response to increasing and decreasing temporal gradients of cAMP that mimic the temporal dynamics of natural waves. The results demonstrate that the *sglA*Δ cells are defective in suppressing lateral pseudopod formation in buffer and during chemotaxis, resulting in defects in basic motile behavior and in a lowered efficiency of chemotaxis in a spatial gradient of cAMP. These defects do not affect either the basic capacity to sense a spatial gradient of cAMP or to respond to the temporal and concentration components of the natural chemotactic wave. The defect in the suppression of lateral pseudopod formation of *sglA*Δ mutants is remarkably similar to that of the myosin I null mutants *myoA*$^-$ and *myoB*$^-$ [Wessels et al., 1991, 1996; Titus et al., 1992; Falk et al., 2003], and the clathrin null mutant [Wessels et al., 2000], suggesting that S-1-P may be involved in modulating these cytoskeletal components in the process of pseudopod formation.

MATERIALS AND METHODS

Strains and Culture Conditions

Strain SA554 is a mutant strain of *Dictyostelium discoideum* in which the gene encoding the enzyme sphingosine-1 phosphate lyase (*sglA*) has been inactivated using the restriction enzyme mediated insertion (REMI) technique (denoted *sglA*Δ (*R*)) [Li et al., 2000]. This mutant was obtained during a selection for mutants that exhibited increased resistance to the chemotherapeutic drug cisplatin. It contains a single insertion in the *sglA* gene. Strain SA555 is a mutant in which the *sglA* gene was inactivated by direct homologous recombination (*sglA*Δ) [Li et al., 2000]. Both mutant strains show increased resistance to cisplatin and exhibit aberrant mor-

phogenesis. Ax4 is the wild-type strain that was the parent of both mutant strains.

Cell cultures in liquid HL-5 medium were initiated on a monthly basis from spores desiccated on silica gel. Development was initiated by washing the cells free of medium with buffered salts solution (BSS: 20 mM KCl, 2.5 mM $MgCl_2$, 40 mM K-PO_4, pH 6.4) [Sussman, 1987] and distributing them on paper filter pads saturated with BSS at a density of 5×10^6 per cm^2 [Soll, 1987]. For all analyses but developmental regulation of cell motility, cells were harvested in BSS at the ripple stage of development, which represents the onset of aggregation [Soll, 1979] and the time at which cells achieve peak velocity [Varnum et al., 1986].

Basic motile behavior. Cells were distributed on the wall of a Sykes-Moore perfusion chamber, positioned on the stage of an upright microscope with long-distance working condenser and a 25× bright-field objective. The chamber was then perfused with buffered salts saturation as previously described [Falk et al., 2003; Wessels et al, 1989; Zhang et al., 2002, 2003]. Cell behavior was continuously videorecorded over a 10-min period for computer-assisted motion analysis.

Behavior in a spatial gradient of cAMP. Cells were dispersed on the bridge of a Plexiglas chemotaxis chamber [Varnum and Soll, 1984] fashioned after that of Zigmond [1977] as previously described [Falk et al., 2003; Wessels et al., 1989; Zhang et al., 2002, 2003]. Buffered salts solution alone was added to one well and buffered salts solution plus 10^{-6} M cAMP to the other well bordering the bridge. After 5 min, cell behavior was videorecorded for a 10-min period for computer-assisted motion analysis.

Behavior in simulated temporal waves of cAMP. Cells were washed from filter pads with buffered salts solution and distributed on the wall of a perfusion chamber. Four temporal waves mimicking the temporal dynamics of a natural wave were generated with NE-1000 Multi-Phaser programmable syringe pumps (New Era Pump Systems, Wantagh, NY) according to methods previously described [Geiger et al., 2003].

2D-DIAS analysis of behavior. DIAS software was used for the computer-assisted analysis of behavior in 2D as previously described in detail [Soll, 1995; Soll and Voss, 1998]. Instantaneous velocity and directional change were computed as previously described [Soll, 1995; Wessels et al., 2004]. Directional persistence was computed as the net distance between the first and last point in a centroid track, divided by total distance of the track. Difference pictures were generated by superimposing the perimeter outline of the cell in frame *n* onto the perimeter outline in frame *n*-1. Expansion zones were regions of the cell in *n* not overlapping the cell in frame *n*-1. The percent of the cell image at *n*-1 that was in an expansion zone at *n* was considered a measure of positive flow. Chemotactic index was measured as the net distance traveled directly towards the well containing chemoattractant divided by total distance. Percent positive chemotaxis was the proportion of cells exhibiting a positive chemotactic index.

3D-DIAS reconstruction. 3D-DIAS software was used to reconstruct live cells at 4-sec intervals according to methods previously described in detail [Wessels et al., 1998, 2004; Soll and Voss, 1998; Heid et al., 2002]. 3D-DIAS software in the newly developed JAVA-based DIAS 4.0 platform (E. Voss and D.R. Soll, unpublished data) automatically outlined the perimeter of the in-focus portion of the image in each optical section using a pixel complexity algorithm [Soll et al., 2000].

F-actin localization. Cells were fixed with 4% paraformaldehyde in 10 nM (2N-morpholins) ethanesulfonic acid (MES; Sigma, St. Louis, MO) buffer (pH 6.1) containing 138 mM KCl, 3 mM $MgCl_2$, and 2 mM EGTA. Cells were then stained with Oregon green-phalloidin (Molecular Probes, Inc.) according to methods previously described [Zhang et al., 2003]. Coverslips were rinsed and mounted using Velvalloy supplemented with 0.6% N-propylgellate (Sigma). Cells were then scanned with a Bio-Rad (Richmond, CA) Radiance 2100MP LSCM at 0.2-μm increments in the z-axis, and the z series projected as a single image.

RESULTS

Developmental Regulation of Cell Motility

Individual cell velocity in the absence of a chemotactic signal has been shown to increase at the onset of aggregation in wild-type *D. discoideum* cells [Varnum et al., 1986]. To test whether cell motility was developmentally regulated in a normal fashion in *sglA*Δ cells, individual cells removed from developing cultures at time intervals were analyzed for mean instantaneous velocity using 2D-DIAS software. The mean instantaneous velocity of individual control Ax4 cells remained between 4 and 5 μm per min for the first 4 h of development, increased to a maximum of 10.6 μm per min at 7 h, coincident with the onset of aggregation, then decreased (Fig. 1). The mean instantaneous velocity of *sglA*Δ cells also remained between 4 and 5 μm per min for the first 4 h of development, then increased to a maximum at 7 h, at the onset of aggregation, as it did in control cells (Fig. 1). However, the peak velocity was 8.2 μm per min, approximately 25% lower than that of control cells ($P < 0.01$) (Fig. 1). Therefore, although the developmental time at which the velocity of individual *sglA*Δ cells peaked was normal, the peak velocity attained was lower than that of control cells. In subsequent computer-assisted comparisons of motility reported here, both control

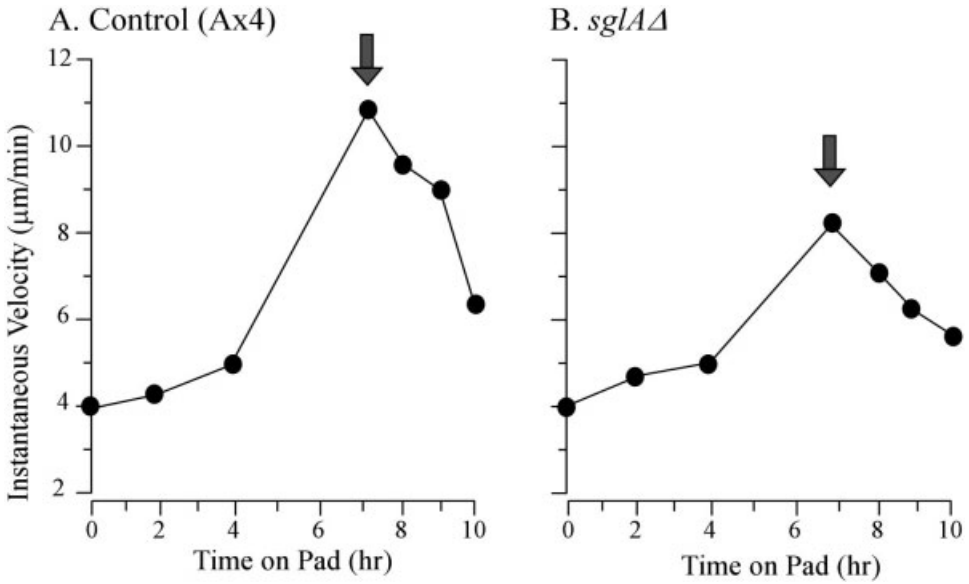

Fig. 1. Motility, assessed by velocity, is developmentally regulated in mutant *sglA*Δ (**B**), as it is in Ax4 control cells (**A**). Cells were developed on filter pads saturated with buffered salts solution. The mean instantaneous velocity was computed from the average instantaneous velocity of 20 individual amoebae analyzed for 10 min at each time point. *Arrows* represent the time at which control and mutant cells were taken for subsequent studies.

TABLE I. 2D-DIAS Analysis of Cell Behavior in Buffer Reveals a Reduction in Velocity for S-1-P Lyase Null Cells

Cell type	Number of cells analyzed	Instantaneous velocity (μm per min)	Positive flow (%/4 sec)	Directional change (deg/4 sec)	Directional persistence (*net dist.* total dist, 10 min)	Roundness (%)
AX4	48	9.8 ± 2.5	10.9 ± 3.2	43.4 ± 10.4	0.36 ± 0.21	52.4 ± 8.2
*sglA*Δ	40	7.6 ± 3.0	10.3 ± 3.5	52.5 ± 11.8	0.21 ± 0.15	57.1 ± 13.4
P values		4×10^{-4}	NS	3×10^{-4}	2×10^{-4}	NS

and mutant *sglA*Δ cells were analyzed at the onset of aggregation.

*sglA*Δ Cells Exhibit Defects in Basic Motile Behavior

To identify the behavioral defects leading to the observed decrease in mean instantaneous velocity, the behavior of *sglA*Δ cells migrating in buffer was compared to that of control cells. As observed in the analysis of cell motility during development (Fig. 1), the mean instantaneous velocity of *sglA*Δ cells, in this more detailed analysis, was approximately 25% lower than that of control cells (Table I). The decrease in mean instantaneous velocity was not, however, accompanied by a decrease in the mean positive flow parameter (Table I), a measure of area displacement computed independently of the cell centroid [Soll, 1995]. This suggested that while *sglA*Δ cells possess protrusive activity similar to that of control cells (measured as positive flow), protrusion may be less organized, and hence may lead to a loss in the efficiency of translocation (measured as instantaneous velocity). This conclusion was supported by measures of mean directional change and mean directional persistence, which were higher and lower, respectively, in *sglA*Δ cells than in control cells (Table I). A comparison of the perimeter tracks of *sglA*Δ and control cells supported this conclusion. The tracks of control cells (Fig. 2A) were longer and included fewer turns than the tracks of *sglA*Δ cells (Fig. 2B). Taken together, these results indicated that mutant cells turned more often, indicating a higher frequency of lateral pseudopod formation. Differential interference contrast (DIC) images of control and *sglA*Δ cells supported this conclusion. While elongate control cells extended on average a single, dominant, compact, anterior pseudopod that contained particulate-free cytoplasm (Fig. 3A–D), elongate *sglA*Δ cells extended on average both a dominant anterior pseudopod and several lateral pseudopods that contained particulate-free cytoplasm (Fig. 3E–H). This abnormal extension of more than one pseudopod at the

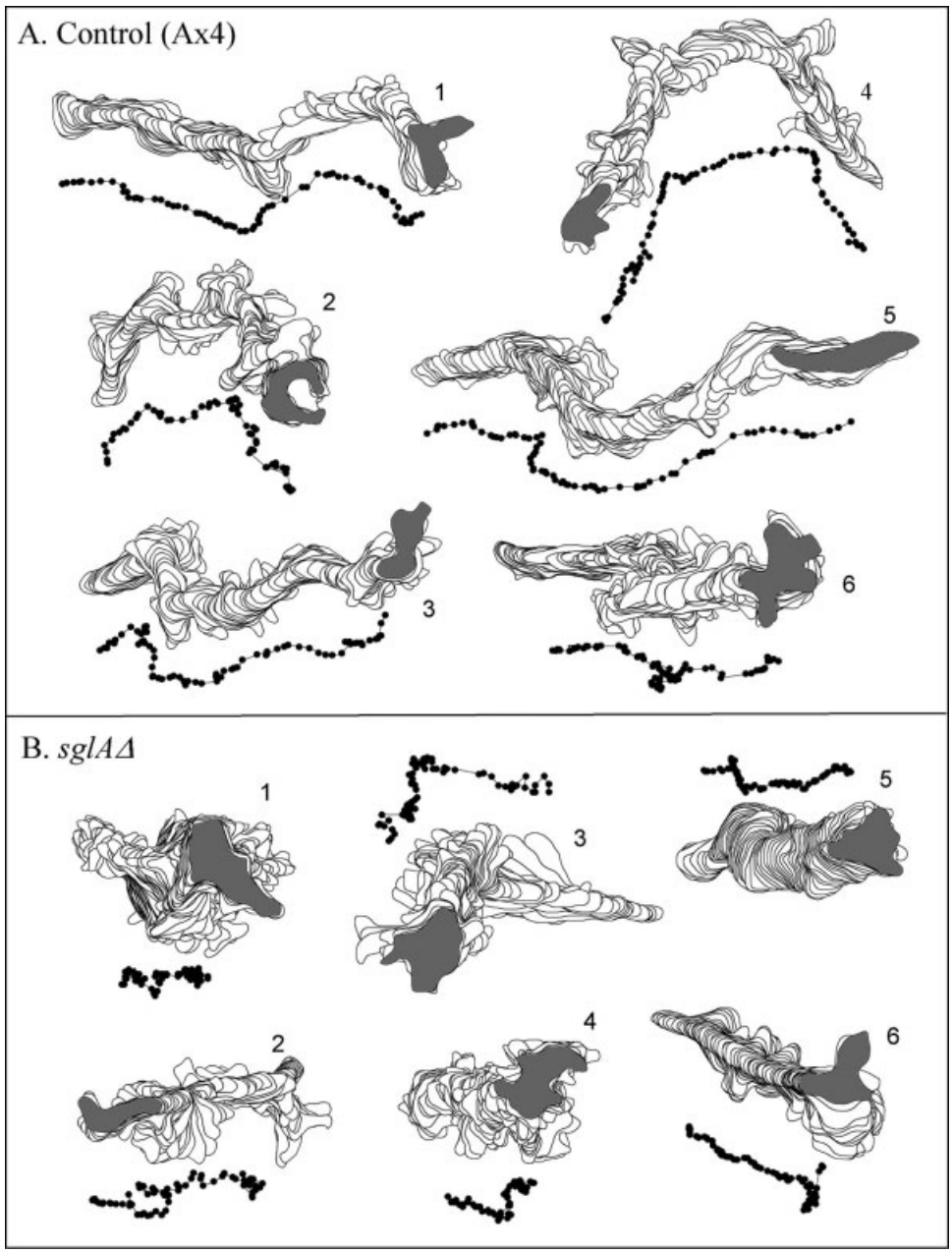

Fig. 2. Computer-generated perimeter and centroid tracks of representative control (**A**) and *sglA*Δ (**B**) cells translocating in buffered salts solution in the absence of chemoattractant revealed slower average velocities and rounder shapes for mutant cells. Cells are numbered. *Gray cell profile* represents last cell outline in each perimeter track. Perimeters were outlined at 8-sec intervals.

same time resulted in a slightly wider cells, as is evident in both perimeter tracks (Fig. 2) and DIC images (Fig. 3). This conclusion was further supported by a mean roundness parameter higher than that of control cells (Table I).

To obtain a more complete view of the morphological abnormalities of *sglA*Δ cells migrating in buffer, 3D reconstructions were generated at 4-sec intervals using 3D-DIAS software [Wessels et al., 1998]. Control cells migrating in buffer were elongate along the substratum, extended on average a single, compact, anterior pseudopod, and possessed an identifiable, tapered uropod (Fig. 4A). *sglA*Δ cells were also on average elongate along the substratum and at times exhibited a tapered uropod (Fig. 4B). However, *sglA*Δ cells abnormally extended multiple pseudopods from the cell periphery (Fig. 4B), as was evident in DIC images (Fig. 3E–H).

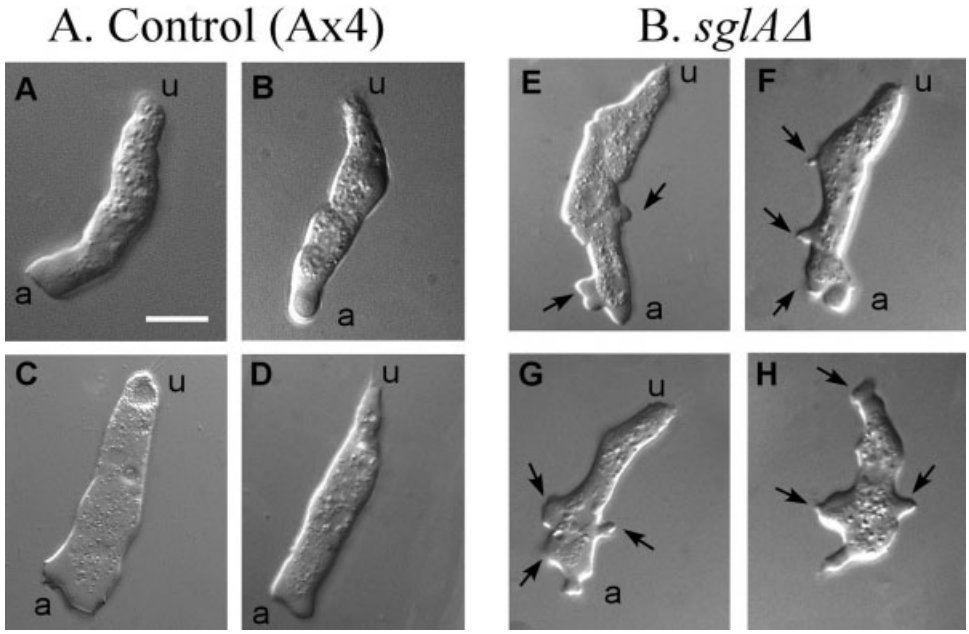

Fig. 3. Differential interference contrast microscopy reveals that *sglA*Δ cells (**B**) translocating in buffered salts solution in the absence of chemoattractant form more lateral pseudopods than control cells (**A**). *Arrows* point to lateral pseudopod extensions. Note that the cytoplasm of both lateral and anterior pseudopods is particulate-free, while that of the main cell body is particulate. u, uropod; a, anterior end of cell. Scale bar = 5 μm.

These multiple pseudopods projected from the sides of the cell along the substratum without regard to the established polarity of the cell, which could be assessed from the centroid track (data not shown).

The behavior in buffer of *sglA*Δ, generated by direct homologous recombination, was compared to that of cells of the null mutant *sglA*Δ (*R*), generated independently by REMI insertional mutagenesis. Like *sglA*Δ, *sglA*Δ (*R*) exhibited a significant reduction in mean instantaneous velocity when compared to control Ax4 cells (8.2 ± 2.8 μm per min for *sglA*Δ (*R*) versus 9.8 ± 2.5 μm per min for control Ax4 cells, $P = 0.0004$). Like *sglA*Δ, *sglA*Δ (*R*) exhibited the same mean positive flow measure as control Ax4 cells (10.3 ± 3.2% per 4 sec for both). In addition, DIC images of translocating *sglA*Δ (*R*) cells revealed an increased frequency of lateral pseudopod formation (data not shown), like *sglA*Δ mutant cells (Fig. 3E–H).

F-Actin Localization

The abnormal pseudopods formed by *sglA*Δ cells were particulate-free (Fig. 3E–H), like normal anterior and lateral pseudopods of control Ax4 cells (Fig. 3A–D). Since normal anterior and lateral pseudopods contain high levels of F-actin, we stained Ax4 and *sglA*Δ cells migrating in buffer with Oregon Green™-conjugated phalloidin, which preferentially binds to F-actin. Cells were imaged with a laser scanning confocal microscope. Scans at 0.2-μm intervals in the z-axis were then stacked. The majority of F-actin localized in anterior (A) and lateral (L) pseudopods of control cells (Fig. 5A–D). The particulate cytoplasm stained diffusely, and the cortex of the cell body exhibited low level localized staining (Fig. 5A–D). Punctate F-actin staining was also observed in the ventral cortex (Fig. 5A–D). The majority of F-actin localized to the anterior as well as to the multiple lateral pseudopods of *sglA*Δ cells. The particulate cytoplasm and cortex of the cell body stained similarly to that of control cells (Fig. 5E–H). Punctate F-actin staining was also observed in the ventral cortex (Fig. 5E–H). These results support and extend the previous fluorescent analysis of F-actin localization in *sglA*Δ [Li et al., 2001], and demonstrate that the multiple lateral pseudopod-like extensions of *sglA*Δ cells contain high levels of f-actin like normal pseudopodia.

Chemotaxis in a Spatial Gradient of cAMP

At the onset of a natural wave of cAMP, cells polarize in the direction of the source of the wave (the aggregation center), in response to the positive spatial gradient of cAMP associated with the front of the wave [Soll et al., 2003]. Polarization involves extension of the dominant pseudopod in the direction of increasing cAMP concentration. Since *sglA*Δ cells exhibit a defect in pseu-

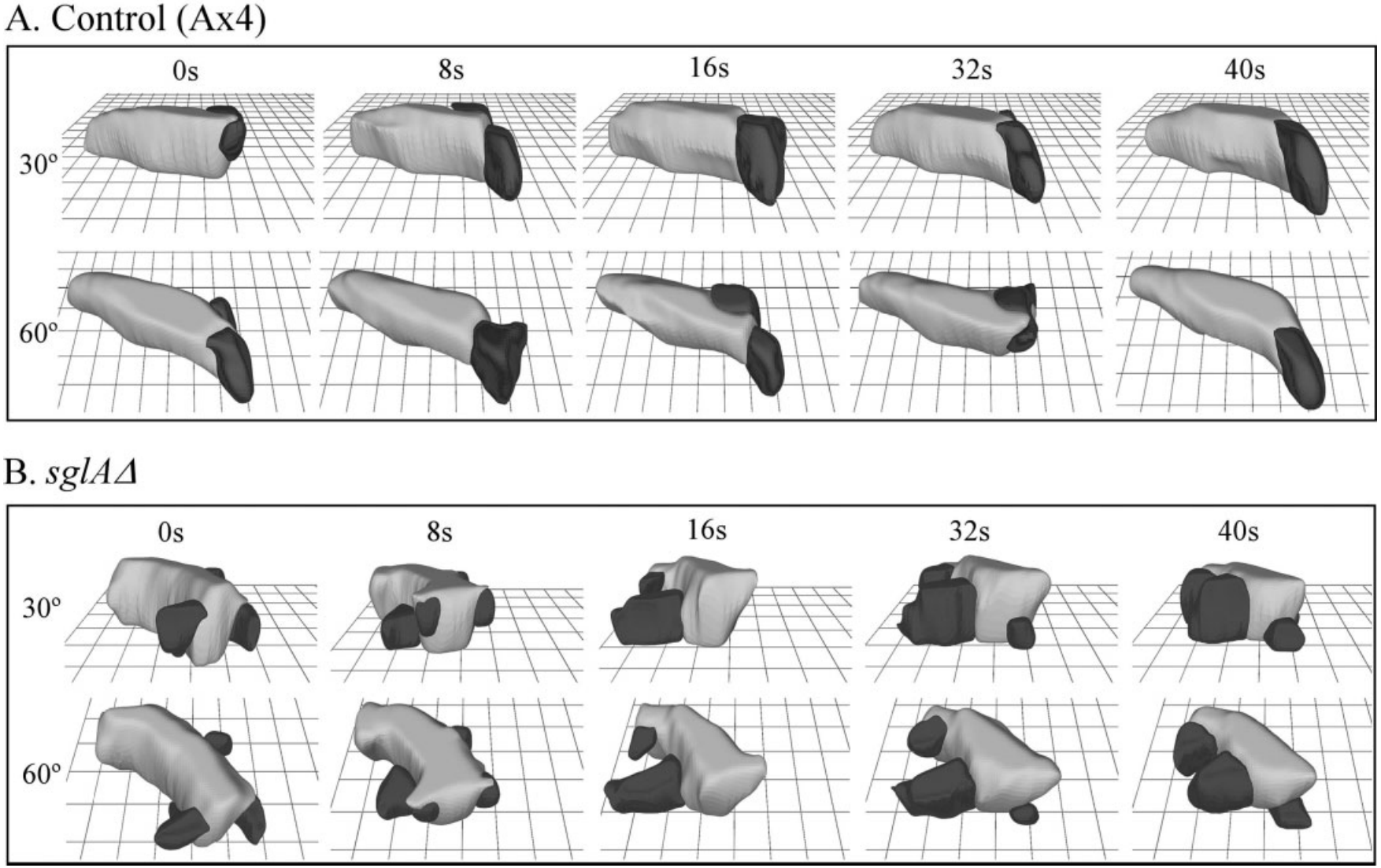

Fig. 4. 3D-DIAS reconstructions of a representative live control (**A**) and *sglA*Δ (**B**) cell migrating in buffered salts solution reveal that mutant cells have a less elongate shape and form more lateral pseudopods. Both cells were reconstructed over a 40-sec (s) period. *Light grey portion* of reconstruction, main cell body; *dark grey portion* of reconstruction, pseudopods.

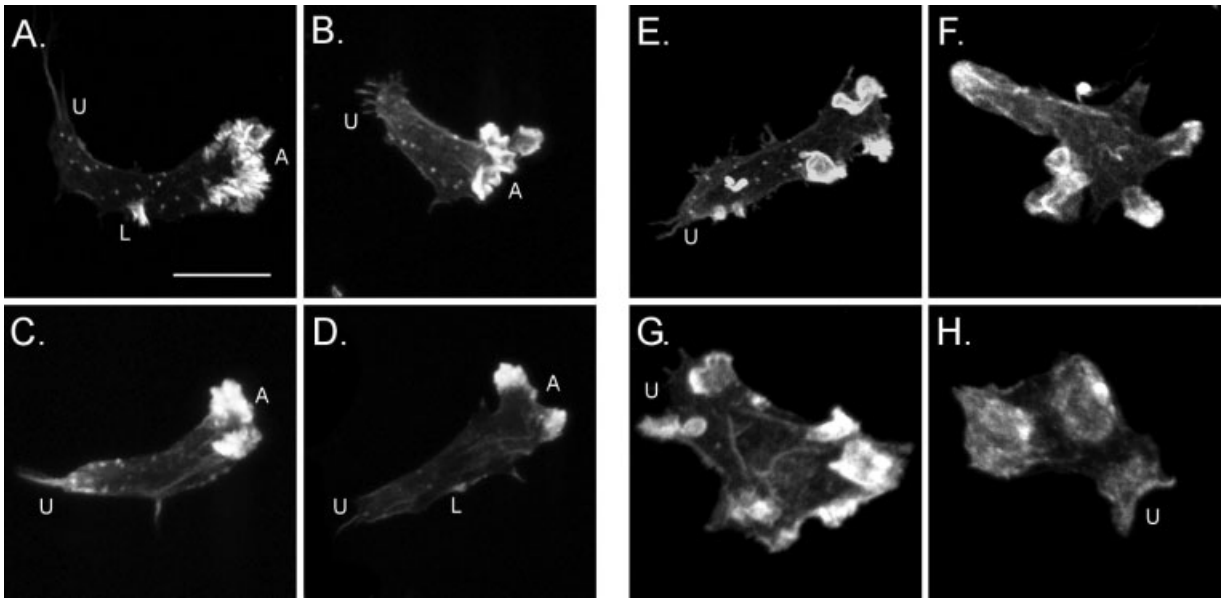

Fig. 5. Staining with Oregon Green-phalloidin reveals that the multiple pseudopods formed by *sglA*Δ cells (**B**) contain high levels of F-actin, just as the dominant pseudopod in control cells (**A**). A, anterior end; U, uropod; L, lateral pseudopod. Scale bar = 5 μm.

TABLE II. 2D-DIAS Analysis of Cell Behavior in a Spatial Gradient of cAMP Reveals That S-1-P Lyase Null Cells Are Chemotactically Less Efficient Than Control Cells, and Exhibit Many of the Same Behavior Defects Exhibited in Buffer

Cell type	Number of cells analyzed	Instantaneous velocity (μm per min)	Positive flow (%/4 sec)	Directional change (deg/4 sec)	Directional persistence (*net dist.* total dist., 10 sec)	Chemotactic index	Percent positive chemotaxis
AX4	48	11.5 ± 4.1	9.7 ± 2.6	33.3 ± 14.2	0.64 ± 0.20	+0.56 ± 0.27	98
*sglA*Δ (*R*)	58	6.7 ± 1.9	8.8 ± 2.8	47.6 ± 10.5	0.34 ± 0.22	+0.21 ± 0.29	84
*sglA*Δ	65	7.8 ± 2.2	10.0 ± 3.4	44.7 ± 9.4	0.34 ± 0.22	+0.14 ± 0.29	71
P value (AX4 *vs sglA*Δ (*R*))		2×10^{-10}	NS	1×10^{-7}	1×10^{-10}	5×10^{-9}	
P value (AX4 *vs sglA*Δ)		4×10^{-9}	NS	6×10^{-7}	1×10^{-10}	2×10^{-11}	

dopod extension in buffer, it was possible that they would also exhibit a defect in chemotaxis. Therefore, the behavior of control cells and cells of both the *sglA*Δ mutant and the *sglA*Δ (*R*) mutant were motion-analyzed in spatial gradients of cAMP generated across the bridge of a gradient chamber.

In a spatial gradient of cAMP, the instantaneous velocity of Ax4 cells (Table II) was higher than in buffer (Table I), but positive flow was similar. Cells of both mutant lines exhibited mean instantaneous velocities in a spatial gradient of cAMP (Table II) that were similar to that in buffer (Table I and previous text), but significantly lower than that of control Ax4 cells in a spatial gradient of cAMP (Table II). In a spatial gradient of cAMP, the instantaneous velocity of *sglA*Δ (*R*) and *sglA*Δ cells were 42 and 32% lower, respectively, than that of Ax4 cells (Table II). Positive flow of cells of both mutants was similar to that of Ax4 cells (Table II), as it was in buffer (Table I), again suggesting that protrusive activity was similar in mutant and control cells. Cells of both mutant strains also exhibited significantly higher mean directional change and significantly lower directional persistence than control cells in a spatial gradient of cAMP (Table II), as was the case in buffer (Table I), suggesting that mutant cells did not adequately suppress lateral pseudopod formation in a spatial gradient of cAMP.

Cells of both mutant strains were capable of chemotaxis in a spatial gradient of cAMP, but in both cases the efficiency of chemotaxis was significantly reduced. While the mean chemotactic index of Ax4 cells was +0.56 ± 0.27, that of *sglA*Δ and *sglA*Δ (*R*) was +0.14 ± 0.29 and +0.21 ± 0.29, respectively (Table II). The distributions of chemotactic indices revealed that while the majority of chemotactic indices of *sglA*Δ and *sglA*Δ (*R*) cells were in the positive range, they were in

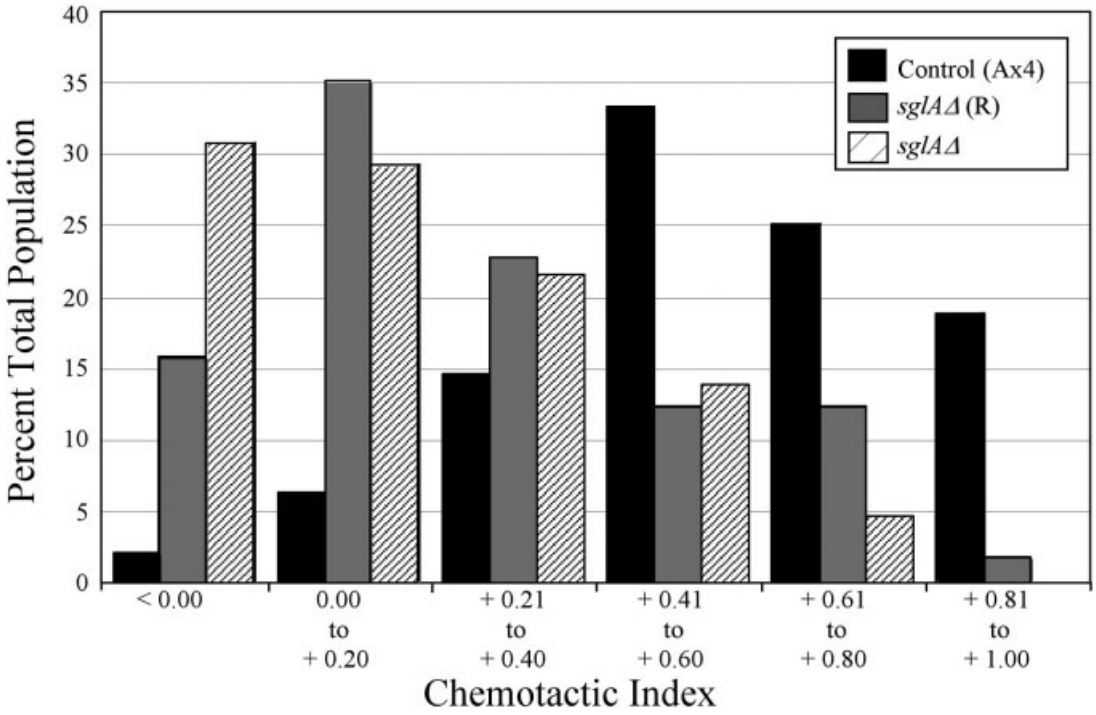

Fig. 6. Histograms of chemotactic indices of cells in spatial gradients of cAMP reveal that fewer *sglA*Δ and *sglA*Δ (*R*) cells, than control cells, exhibit high-end (+0.41 to +1.00) chemotactic indices.

the lower portion of this range (Fig. 6). While 19% of Ax4 cells exhibited chemotactic indices of +0.81 to 1.00, 0% of *sglA*Δ and 2% of *sglA*Δ (*R*) cells were in that high range (Fig. 6). These results suggested that mutant cells were capable of chemotaxis in a spatial gradient of cAMP, but chemotaxis was highly inefficient. Perimeter and centroid tracks supported this interpretation. While the perimeter tracks of Ax4 cells were highly oriented in the direction of increasing cAMP, with few turns (Fig. 7A), the tracks of *sglA*Δ cells, although generally oriented in the correct direction, were far less persistent, far more compact, and included more turns on average (Fig. 7B).

Since the basic behavioral defects revealed by the 2D-DIAS analysis of *sglA*Δ cells in a spatial gradient of cAMP were similar to those in buffer, we tested whether they were also due in part to aberrant pseudopod formation by reconstructing cells in 3D using 3D-DIAS software. While Ax4 cells translocating up a spatial gradient of cAMP were elongate and extended a single dominant anterior, compact pseudopod along the substratum (Fig. 8A), *sglA*Δ cells translocating up a spatial gradient of cAMP were less elongate, extended an anterior pseudopod of a far more complex shape, and continuously extended lateral pseudopods (Fig. 8B). The defects were similar to those revealed in 3D reconstructions of mutant cells migrating in buffer (Fig. 4B).

Responses to Temporal Waves of cAMP

After orientation in response to the positive spatial gradient of cAMP at the onset of the front of the natural wave, the behavioral changes in the remaining front, at the peak and in the back of the wave, are in response to the temporal and concentration components of the wave [Soll et al., 2003]. In response to the increasing temporal gradient of cAMP in the front of the wave, wild-type cells surge towards the aggregation center. In response to the high concentration of cAMP at the peak of the wave and to the decreasing temporal gradient of cAMP in the back of the wave, velocity is suppressed. To test whether these responses were intact in the *sglA*Δ mutant, cells were treated with four temporal waves of cAMP that mimicked the temporal dynamics of natural waves. These waves were generated in a perfusion chamber in the absence of spatial gradients. As previously reported [Varnum et al., 1985; Wessels et al., 1992; Zhang et al., 2002], control cells (N = 10) exhibited velocity surges in the last three in a series of four temporal waves of cAMP (Fig. 9A). *sglA*Δ cells (N = 10) underwent similar velocity surges (Fig. 9B).

DISCUSSION

S-1-P and other sphingolipids have been demonstrated to play important roles in cellular signaling. Con-

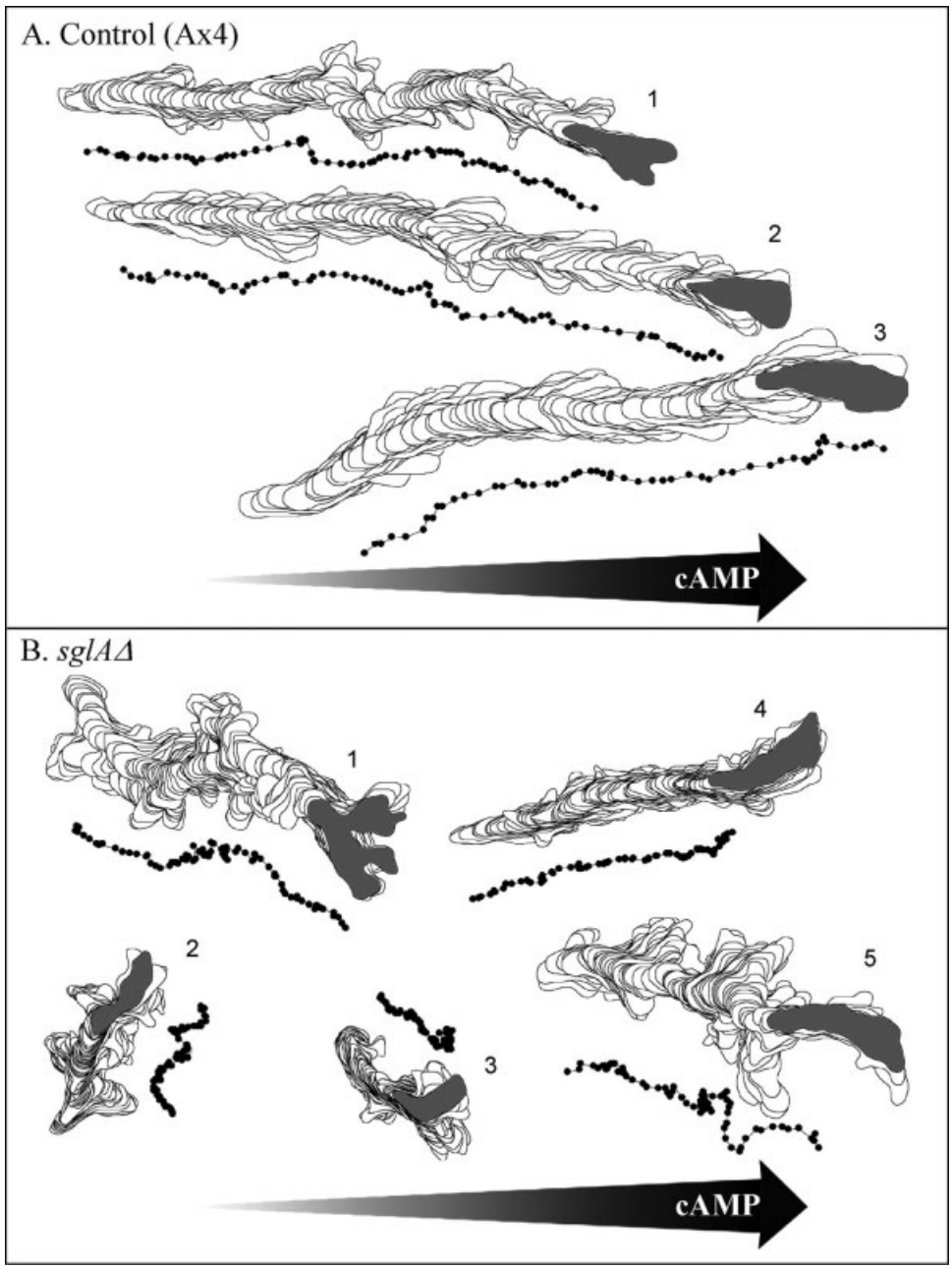

Fig. 7. Computer-generated perimeter and centroid tracks of control (**A**) and *sglA*Δ (**B**) cells translocating in spatial gradients of cAMP reveal that although mutant cells are chemotactically responsive, their tracks include more lateral pseudopod projections and more turns due to the projections, lowering the efficiency of chemotaxis. *Gray cell profile* represents last cell outline in each perimeter track. *Large arrow* points in the direction of the increasing spatial gradient of cAMP.

siderable evidence suggests that S-1-P is unique, functioning both extracellularly as a ligand for a family of G-protein coupled EDG/S1P receptors and intracellularly as a second messenger [Spiegel and Milstien, 2000]. Studies of several model organisms support the idea that S-1-P plays a major role in cell differentiation and morphogenesis. In addition to a role in controlling cell proliferation and cell death, the release of Ca^{2+} stores and gene expression, S-1-P has been implicated in regulating cell motility and chemotaxis in several cultured mammalian cell types [see Spiegel et al., 2002]. Previous work on the role of S-1-P in the development of *D. discoideum* suggested that *sglA*Δ cells were defective in pseudopod formation [Li et al., 2001]. This suggested that they

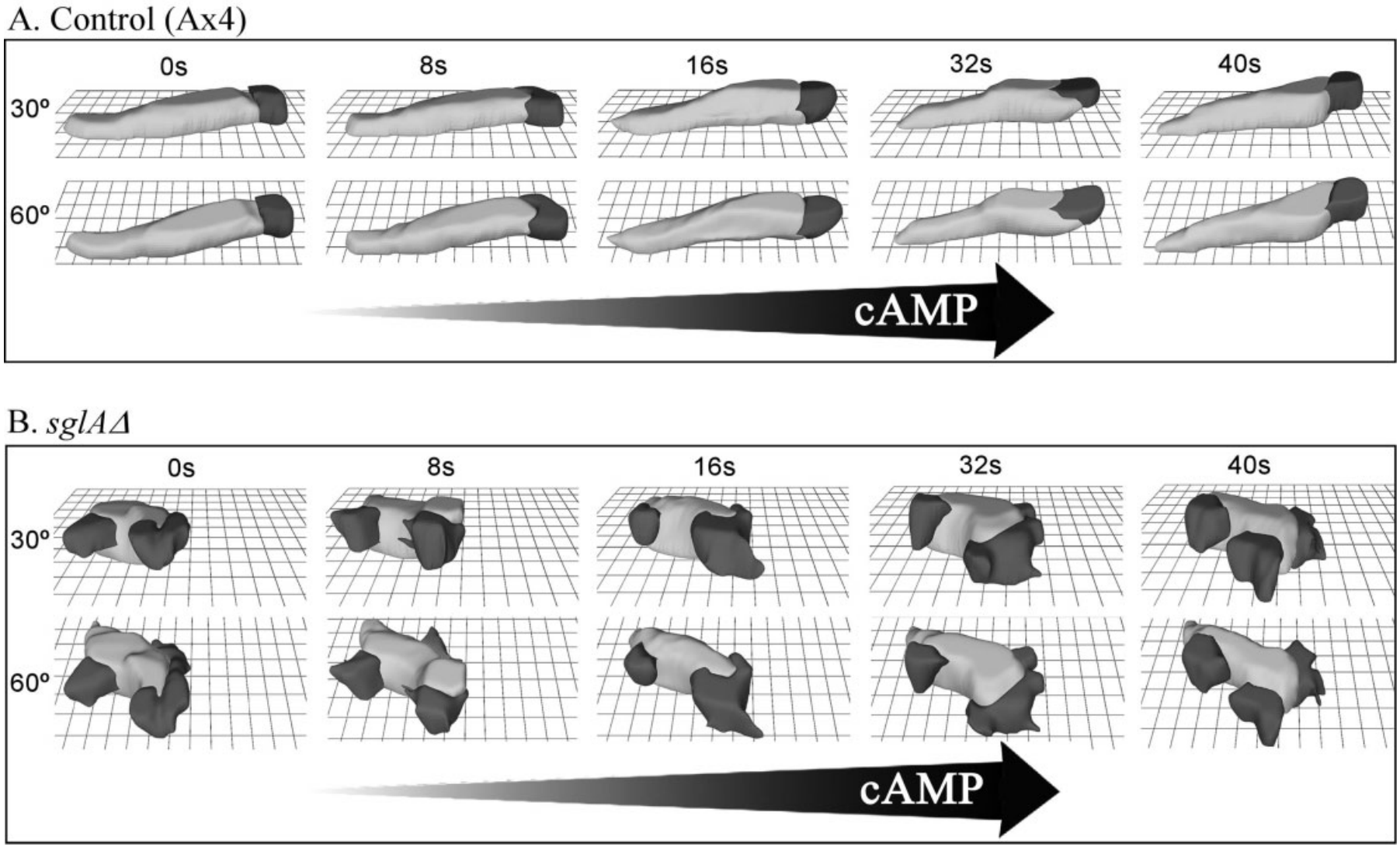

Fig. 8. 3D-DIAS reconstructions of a representative control (**A**) and *sglA*Δ (**B**) cell migrating up a spatial gradient of cAMP reveal that mutant cells are rounder and continue to form lateral pseudopod, in contrast to the control, which has suppressed lateral pseudopod formation. Both cells were reconstructed over a 40-sec (s) period. *Large arrow* points in the direction of increasing spatial gradient of cAMP.

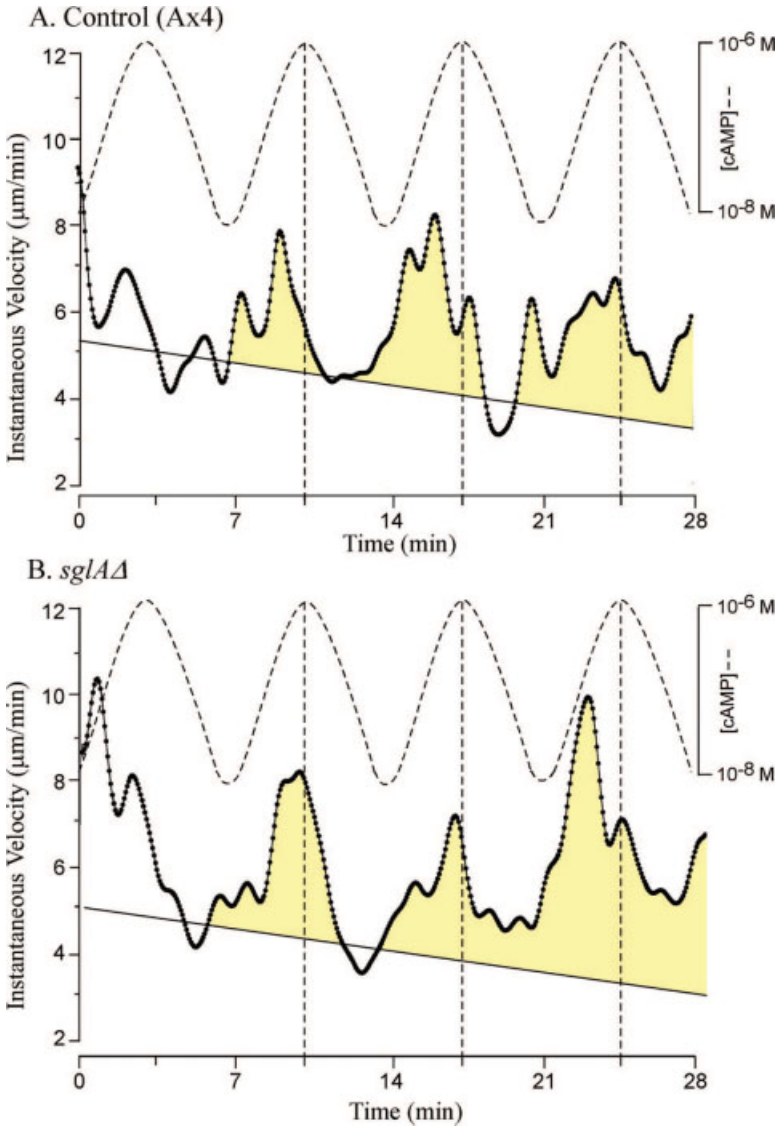

Fig. 9. *sglA*Δ cells (**B**) exhibit velocity surges like control cells (**A**) in the front of the last three in a series of four temporal waves of cAMP generated in a perfusion chamber. Instantaneous velocity plots were smoothed 10 times with Tukey windows of 10, 20, 40, 20, and 10.

TABLE III. The S-1-P Lyase Null Cells, the Class I Myosin A Null Mutant *myoA*$^-$, the Class I Myosin B Null Mutant *myoB*$^-$, and the Clathrin Null Mutant *chc*$^-$ Have the Same Behavioral Phenotypes*

	In buffer		In spatial gradient of cAMP			Response to increasing temporal gradient of cAMP
Mutant	Multiple lateral pseudopods	Decrease in instantaneous velocity (%)	Multiple lateral pseudopods	Decrease in instantaneous velocity (%)	Decrease in chemotactic index (%)	
*sglA*Δ(*R*)	+	−22	+	−33	−63	+
sglA	+	−18	+	−24	−75	+
myoA$^-$	+	−34	+	−22	−52	+
myoB$^-$	+	−24	+	−49	−59	+
chc$^-$	+	−36	+	−48	−68	nd

*The results for *myoA*$^-$ and *myoB*$^-$ were obtained from Falk et al. [2003] and for *chc*$^-$ from Wessels et al. [2000].

would also be defective in some aspect of cell motility and chemotaxis.

Here we analyzed the role of S-1-P in cell motility and chemotaxis by characterizing *D. discoideum* S-1-P lyase mutants using 2D and 3D computer-assisted methods. We have discovered a basic motility defect that is exhibited by *sglA*Δ cells in the absence of chemoattractant and during chemotaxis. *sglA*Δ cells are defective in

suppressing lateral pseudopod formation. This defect results in a decrease in velocity accompanied by an increase in sharp turns and a decrease in the persistence of translocation. This decrease in velocity is not accompanied by a decrease in positive flow, a measure of cellular protrusion computed independently of cell centroid dynamics. Hence, the decrease in velocity is not due to a decrease in protrusive activity per se, but rather a decrease in the localization of protrusions to the anterior end of the cell. The multiple lateral pseudopods extended by *sglA*Δ cells contained particulate-free cytoplasm and concentrated F-actin, both characteristics of true pseudopodia. The expression of this defect in a spatial gradient of cAMP resulted in a dramatic decrease in the efficiency of chemotaxis. *sglA*Δ cells were capable of chemotaxing in spatial gradients of cAMP and responding correctly to the increasing and decreasing gradients of cAMP associated with the front and back of the wave, respectively. However, the mutation resulted in a loss of efficiency both in basic translocation and chemotaxis.

The decreased motility observed in the *D. discoideum* lacking the enzyme responsible for degrading S-1-P to hexadecanal and phosphoethanolamine resembles the defect caused by the addition of S-1-P in cancer cells. S-1-P-treated mammalian cancer cells exhibit lowered levels of motility and chemoinvasivness. These effects are presumed to function through an S-1-P surface receptor. However, in the case of *D. discoideum*, it seems likely that the effect is intracellular since there are no obvious homologs of the EDG/S1P receptors encoded in the *D. discoideum* genome.

We assume that the behavioral defects of *sglA*Δ cells are the result of increased S-1-P levels due to the absence of S-1-P lyase. Although we have not been able to measure S-1-P levels in *D. discoideum*, we have begun to analyze a mutant that overexpresses one of the two *D. discoideum* sphingosine kinase genes (*sgkA*). Sphingosine kinase is the enzyme responsible for synthesizing S-1-P from sphingosine and ATP. This mutant (*sgkAOE*) has a 13-fold increase in sphingosine kinase activity (Alexander and Alexander, unpublished observation). An analysis of the basic cell behavior of *sgkAOE* cells in buffer revealed that these cells, like *sglA*Δ cells, are defective in suppressing lateral pseudopod formation (Wessels et al., unpublished observations), supporting our conclusion that the behavioral defects of *sglA*Δ cells are due to increased S-1-P levels.

The defect in lateral pseudopod suppression and its impact on the translocation and chemotaxis of *sglA*Δ cells are surprisingly similar to the behavioral defects of the two class I myosin mutants, *myoA*$^-$ and *myoB*$^-$ [Falk et al., 2003], and the clathrin null mutant *chc*$^-$ [Wessels et al., 2000]. In buffer, these latter mutants abnormally form multiple lateral pseudopods and exhibit a similar decrease in mean instantaneous velocity, similar to the defects of *sglA*Δ cells (Table III). In a spatial gradient of cAMP, these mutants abnormally form multiple lateral pseudopods, and exhibit a decrease in mean instantaneous velocity and a decrease in average chemotactic index, the same defects exhibited by *sglA*Δ cells (Table III). Finally, *sglA*Δ and the mutants *myoA*$^-$ and *myoB*$^-$ respond normally to an increasing temporal gradient of cAMP in the front of a temporal wave with a surge in velocity (Table III). *chc*$^-$ cells were never tested for this last capability [Wessels et al., 2000]. The similarity in the behavioral defects of the four mutants *myoA*$^-$ *myoB*$^-$, *chc*$^-$, and *sglA*Δ suggests that they are all involved in the same aspect of motility, namely the suppression of lateral pseudopods, a necessary component of the basic motile behavior of a chemotaxing cell [Soll et al., 2003]. These four genes function as a negative regulator of a fine-tuned process. In buffer, normal cells form lateral pseudopods on and off the substratum, and turn into those pseudopods that contact the substratum [Wessels et al., 1994, 1996]. The regulation of lateral pseudopod formation plays a role in chemotaxis in a spatial gradient of cAMP since the frequency of lateral pseudopod formation decreases in direct proportion to the accuracy of orientation in the gradient [Varnum-Finney et al., 1987b]. While these four genes are involved in the negative regulation of lateral pseudopod formation, there must be genes that are involved in the positive regulation of this process, such as those contributing to the Arp2/3-complex (Steiner et al., unpublished observations).

The conclusion that the SglA, MyoA, MyoB, and Chc proteins are all involved in the repression of lateral pseudopod formation is based upon the similarity of individual mutant phenotypes. Epistatic, or other data, are not available for assessing the individuality of function. Because S-1-P functions as a signal, while MyoA, MyoB, and Chc play more mechanistic roles in cellular functions, one might suggest that S-1-P functions upstream of the MyoA, MyoB, and Chc proteins. Since the suppression of lateral pseudopod formation plays such an important role in both chemotaxis in a spatial gradient of cAMP and in the response to the increasing temporal gradient of cAMP associated with the front of the chemotactic wave [Varnum-Finney et al., 1987a; Wessels et al., 1992; Soll et al., 2003], it is possible that SglA, MyoA, MyoB, and Chc are regulated by signals emanating from the spatial, temporal, and concentration components of the natural wave.

Null mutants of *regA*, the gene encoding the cytoplasmic cAMP phosphodiesterase [Wessels et al., 2000], *pkaR*, the gene encoding the regulatory subunit of PKA [Zhang et al., 2000], and *acaA*, the gene encoding ade-

nylate cyclase A (Stepanovic et al., unpublished data), are also defective in suppressing lateral pseudopods. However, their defect is exclusively in response to the chemotactic signal. These mutants migrate and suppress lateral pseudopods in a normal fashion in buffer, in contrast to *myoA*$^-$, *myoB*$^-$, *chc*$^-$ and *sglA*Δ. The mutants *regA*$^-$, *pkAR*$^-$, and *acaA*$^-$ fail to suppress lateral pseudopod formation in response to a spatial or temporal gradient of cAMP. In marked contrast, cells of the mutant S13A, which contains a myosin II regulatory light chain that mimics the constitutively unphosphorylated state [Ostrow et al., 1994], are faster than control cells in buffer and extend fewer lateral pseudopods per unit time than control cells under all conditions, a phenotype opposite that of *sglA*Δ. In a spatial gradient of cAMP, S13A cells are even better at suppressing lateral pseudopods and are chemotactically more efficient than control cells, again a phenotype opposite that of *sglA*Δ. These results suggest that while MyoA, MyoB, Chc, and SglA play roles in the negative regulation of lateral pseudopod formation in the absence of a chemotactic signal, myosin II regulatory light chain phosphorylation plays a role in the positive regulation of lateral pseudopod extension in the absence of a chemotactic signal. In contrast, regA, pkA, and aca play roles in the suppression of lateral pseudopods only in response to a chemotactic signal. Perhaps it is most interesting that all of these genes are involved in the regulation of lateral pseudopod formation and, hence, underscore the importance regulating lateral pseudopod formation plays in motility and chemotaxis.

ACKNOWLEDGMENTS

This work was supported by NIH grant HD-18577 (D.R.S.) and NIH GM53929 (S.A.).

REFERENCES

Boguslawski G, Grogg JR, Welch Z, Ciechanowicz S, Sliva D, Kovala AT, P McGlynn P, Brindley DN, Rhoades RA, English D. 2002. Migration of vascular smooth muscle cells induced by sphingosine 1-phosphate and related lipids: potential role in the angiogenic response. Exp Cell Res 274:264–274.

Bornfeldt KE, Graves LM, Raines EW, Igarashi Y, Wayman G, Yamamura S, Yatomi Y, Sidhu JS, Krebs EG, Hakomori S, et al. 1995. Sphingosine-1-phosphate inhibits PDGF-induced chemotaxis of human arterial smooth muscle cells: spatial and temporal modulation of PDGF chemotactic signal transduction. J Cell Biol 130:193–206.

Cuvillier O, Levade T. 2001. Sphingosine 1-phosphate antagonizes apoptosis of human leukemia cells by inhibiting release of cytochrome c and Smac/DIABLO from mitochondria. Blood 98:2828–2836.

Cuvillier O, Pirianov G, Kleuser B, Vanek PG, Coso OA, Gutkind S, Spiegel S. 1996. Suppression of ceramide-mediated programmed cell death by sphingosine-1- phosphate. Nature 381: 800–803.

DeLozanne A, Spudich JA. 1987. Disruption of the *Dictyostelium* myosin heavy chain gene by homologous recombination. Science 236:1086–1091.

Falk D, Wessels D, Jenkins L, Pham T, Kuhl S, Titus MA, Soll DR. 2003. Shared , unique, and redundant functions of three members of the class I myosins (MyoA, MyoB, and MyoF) in motility and chemotaxis in *Dictyostelium*. J Cell Sci 116:3985–3999.

Firtel RA, Chung CY. 2000. The molecular genetics of chemotaxis: Sensing and responding to chemoattractant gradients. BioEssays 22:603–615.

Geiger J, Wessels D, Soll DR. 2003. Human PMNs respond to temporal waves of chemoattractant like *Dictyostelium*. Cell Motil Cytoskeleton 56:27–44.

Heid P, Voss E, Soll DR. 2002. 3D-DIASemb: a computer-assisted system for reconstructing and motion analyzing in 4D every cell and nucleus in a developing embryo. Dev Biol 245:329–347.

Kessin RH. 2001. *Dictyostelium*: evolution, cell biology, and the development of multicellularity. Cambridge, UK: Cambridge University Press.

Kimura T, Watanabe T, Sato K, Kon J, Tomura H, Tamama K, Kuwabara A, Kanda T, Kobayashi I, Ohta H, Ui M, Okajima F. 2000. Sphingosine 1-phosphate stimulates proliferation and migration of human endothelial cells possibly through the lipid receptors, Edg-1 and Edg-3. Biochem J 348:71–76.

Kuspa A, Loomis WF. 1994. Transformation of *Dictyostelium*: gene disruptions, insertional mutagenesis, and promoter traps. Methods Mol Genet 3:3–21.

Laub M, Loomis WF. 1998. A molecular network that produces spontaneous oscillations in excitable cells of *Dictyostelium*. Mol Biol Cell 9:3521–3532.

Lee OH, Kim YM, Lee YM, Moon EJ, Lee DJ, Kim JH, Kim KW, Kwon YG. 1999. Sphingosine 1-phosphate induces angiogenesis: its angiogenic action and signaling mechanism in human umbilical vein endothelial cells. Biochem Biophys Res Commun 264:743–750.

Li G, Foote C, Alexander S, Alexander H. 2001. Sphingosine-1-phosphate lyase has a central role in the development of *Dictyostelium discoideum*. Development 128:3473–3483.

Li GC, Alexander H, Schneider N, Alexander S. 2000. Molecular basis for resistance to the anticancer drug cisplatin in *Dictyostelium*. Microbiology 146:2219–2227.

Machwate M, Rodan SB, Rodan GA, Harada SI. 1998. Sphingosine kinase mediates cyclic AMP suppression of apoptosis in rat periosteal cells. Mol Pharmacol 54:70–77.

Okamoto H, Takuwa N, Gonda K, Okazaki H, Chang K, Yatomi Y, Shigematsu H, Takuwa Y. 1998. EDG1 is a functional sphingosine-1-phosphate receptor that is linked via a Gi/o to multiple signaling pathways, including phospholipase C activation, Ca2+ mobilization, Ras-mitogen-activated protein kinase activation, and adenylate cyclase inhibition. J Biol Chem 273: 27104–27110.

Okamoto H, Takuwa N, Yokomizo T, Sugimoto N, Sakurada S, Sigematsu H, Takuwa Y. 2000. Inhibitory regulation of Rac activation, membrane ruffling, and cell migration by the G protein-coupled sphingosine-1-phosphate receptor EDG5 but not EDG1 or EDG3. Mol Cell Biol 20:9247–9261.

Ostrow BD, Chen P, Chisholm R. 1994. Expression of a myosin regulatory light chain phosphorylation site mutant complements the cytokinesis and developmental defects of *Dictyostelium* RMLC null cells. J Cell Biol 127:1945–1955.

Pyne S, Pyne NJ. 1996. The differential regulation of cyclic AMP by sphingomyelin-derived lipids and the modulation of sphingolipid-stimulated extracellular signal regulated kinase-2 in airway smooth muscle. Biochem J 315:917–923.

Pyne S, Pyne NJ. 2000. Sphingosine 1-phosphate signalling in mammalian cells. Biochem J 349:385–402.

Saba JD, Hla T. 2004. Point-counterpoint of sphingosine 1-phosphate metabolism. Circul Res 94:724–734.

Sadahira Y, Ruan F, Hakomori S, Igarashi Y. 1992. Sphingosine 1-phosphate, a specific endogenous signaling molecule controlling cell motility and tumor cell invasiveness. Proc Natl Acad Sci USA 89:9686–9690.

Sliva D, Mason R, Xiao H, English D. 2000. Enhancement of the migration of metastatic human breast cancer cells by phosphatidic acid. Biochem Biophys Res Commun 268:471–479.

Soll DR. 1979. Timers in developing systems. Science 203:841–849.

Soll DR. 1987. Methods for manipulating and investigating developmental timing in *Dictyostelium discoideum*. In: Spudich J, editor. Methods in cell biology. New York: Academic Press. p 413–431.

Soll DR. 1995. The use of computers in understanding how cells crawl. Int Rev Cytol 163:43–104.

Soll DR, Voss E. 1998. Two and three dimensional computer systems for analyzing how cells crawl. In: Soll DR, Wessels D, editors. Motion analysis of living cells. New York: John Wiley, Inc. p 25–52.

Soll DR, Voss E, Johnson O, Wessels D. 2000. Three-dimensional reconstruction and motion analysis of living, crawling cells. Scanning 22:249–257.

Soll DR, Wessels D, Zhang H, Heid P. 2003. A contextual framework for interpreting the roles of proteins in motility and chemotaxis in *Dictyostelium discoideum*. J Musc Res Cell Motil 23:659–672.

Spiegel S. 1999. Sphingosine 1-phosphate: a prototype of a new class of second messengers. J Leukoc Biol 65:341–344.

Spiegel S. 2000. Sphingosine 1-phosphate: a ligand for the EDG-1 family of G-protein-coupled receptors. Ann N Y Acad Sci 905:54–60.

Spiegel S, Milstien S. 2000a. Functions of a new family of sphingosine-1-phosphate receptors. Biochim Biophys Acta 1484: 107–116.

Spiegel S, Milstien S. 2000b. Sphingosine-1-phosphate: signaling inside and out. FEBS Lett 476:55–57.

Spiegel S, Milstien S. 2002. Sphingosine 1-phosphate, a key cell signaling molecule. J Biol Chem 277:25851–25854.

Spiegel S, English D, Milstien S. 2002. Sphingosine 1-phosphate signaling: providing cells with a sense of direction. Trends Cell Biol 12:236–242.

Sussman M. 1987. Cultivation and synchronous morphogenesis of *Dictyostelium* under controlled experimental conditions. Methods Cell Biol 28:9–29.

Titus M, Wessels D, Spudich J, Soll DR. 1992. The unconventional myosin encoded by the *myoA* gene plays a role in *Dictyostelium* motility. Mol Biol Cell 4:233–246.

Van Brocklyn JR, Lee MJ, Menzeleev R, Olivera A, Edsall L, Cuvillier O, Thomas DM, Coopman PJ, Thangada S, Liu CH, Hla T, Spiegel S. 1998. Dual actions of sphingosine-1-phosphate: extracellular through the Gi- coupled receptor Edg-1 and intracellular to regulate proliferation and survival. J Cell Biol 142: 229–240.

Varnum B, Soll DR. 1984. The effects of cAMP on single cell motility in *Dictyostelium*. J Cell Biol 99:1151–1155.

Varnum B, Edwards K, Soll DR. 1985. *Dictyostelium* amebae alter motility differently in response to increasing versus decreasing temporal gradients of cAMP. J Cell Biol 101:1–5.

Varnum B, Edwards K, Soll DR. 1986. The developmental regulation of single cell motility in *Dictyostelium discoideum*. Dev Biol 113:218–227.

Varnum-Finney B, Edwards K, Voss E, Soll DR. 1987a. Amoebae of *Dictyostelium discoideum* respond to an increasing temporal gradient of the chemoattractant cAMP with a reduced frequency of turning: evidence for a temporal mechanism in amobeoid chemotaxis. Cell Motil Cytoskeletom 8:7–17.

Varnum-Finney B, Voss E, Soll DR. 1987b. Frequency and orientation of pseudopod formation of *Dictyostelium discoideum* amoebae chemotaxing in a spatial gradient: further evidence for a temporal mechanism. Cell Motil Cytoskeleton 8:18–26.

Wang F, Nohara K, Olivera A, Thompson EW, Spiegel S. 1999. Involvement of focal adhesion kinase in inhibition of motility of human breast cancer cells by sphingosine 1-phosphate. Exp Cell Res 247:17–28.

Wessels D, Schroeder N, Voss E, Hall A, Condeelis J, Soll DR. 1989. cAMP mediated inhibition of intracellular particle movement and actin reorganization in *Dictyostelium discoideum*. J Cell Biol 101:2841–2851.

Wessels D, Murray J, Hammer J, Soll DR. 1991. Myosin IB null mutant of *Dictyostelium* exhibits abnormalities in motility. Cell Motil Cytoskeleton 20:301–315.

Wessels D, Murray J, Soll DR. 1992. Behavior of *Dictyostelium* amoebae is regulated primarily by the temporal dynamic of the natural cAMP wave. Cell Motil Cytoskeleton 23:145–156.

Wessels D, Vawter-Hugart H, Murray J, Soll DR. 1994. 3-dimensional dynamics of pseudopod formation and the regulation of turning during the motility cycle of *Dictyostelium*. Cell Motil Cytoskeleton 41:225–246.

Wessels D, Titus M, Soll DR. 1996. A *Dictyostelium* myosin I plays a crucial role in regulating the frequency of pseudopods formed on the substratum. Cell Motil Cytoskeleton 33:64–79.

Wessels D, Voss E, Von Bergen N, Burns R, Stites J, Soll DR. 1998. A computer-assisted system for reconstructing and interpreting the dynamic three-dimensional relationships of the outer surface, nucleus and pseudopods of crawling cells. Cell Motil Cytoskeleton 41:225–246.

Wessels D, Reynolds J, Johnson O, Voss E, Burns R, Daniels K, Gerrard E, O'Halloran T, Soll DR. 2000. Clathrin plays a novel role in the regulation of cell polarity, pseudopod formation, uropod stability and motility in *Dictyostelium*. J Cell Sci 113:21–36.

Wessels D, Brincks R, Kuhl S, Stepanovic V, Daniels KJ, Weeks G, Lim CJ, Fuller D, Loomis WF, Soll DR. 2004. RasC plays a selective role in the transduction of temporal gradient information in the cAMP wave of *Dictyostelium*. Euk Cell 3:646–662.

Wu J, Spiegel S, Sturgill TW. 1995. Sphingosine 1-phosphate rapidly activates the mitogen-activated protein kinase pathway by a G protein-dependent mechanism. J Biol Chem 270:11484–11488.

Yamamura S, Sadahira Y, Ruan F, Hakomori S, Igarashi Y. 1996. Sphingosine-1-phosphate inhibits actin nucleation and pseudopodium formation to control cell motility of mouse melanoma cells. FEBS Lett 382:193–197.

Yamamura S, Yatomi Y, Ruan F, Sweeney EA, Hakomori S, Igarashi Y. 1997. Sphingosine 1-phosphate regulates melanoma cell motility through a receptor-coupled extracellular action and in a pertussis toxin-insensitive manner. Biochemistry 36:10751–10759.

Zhang H, Wessels D, Fey P, Daniels K, Chisholm R, Soll DR. 2002. Phosphorylation of the myosin regulatory light chain plays a role in cell motility and polarity during *Dictyostelium* chemotaxis. J Cell Sci 115:1733–1747.

Zhang H, Heid P, Wessels D, Daniels K, Pham T, Loomis WF, Soll DR. 2003. Constitutively active protein kinase A disrupts motility and chemotaxis in *Dictyostelium discoideum*. Euk Cell 2:62–75.

Zigmond SH. 1977. The ability of polymorphonuclear leukocytes to orient in gradients of chemotactic factors. J Cell Biol 75:606–616.